

Auger recombination in narrow-gap semiconductor superlattices

B. Vinter*

THALES Research and Technology, Domaine de Corbeville, F-91404 Orsay CEDEX, France

(Received 28 February 2002; published 31 July 2002)

An extended $k \cdot p$ formalism has been developed to describe wave functions in narrow-band-gap semiconductors and narrow-band-gap superlattices. The model shows very satisfactory agreement with various experimental results such as optical absorption spectra in both bulk narrow-gap semiconductors and in narrow-gap superlattices. Based on the model we calculate the Auger recombination rates in InAsSb alloys and in InAsSb-based superlattices. We demonstrate that the Auger recombination coefficient of the superlattices may be larger or smaller than that of bulk alloys of similar gaps depending on the superlattice structure. From the study of several structures we propose a design strategy for minimizing the Auger recombination.

DOI: 10.1103/PhysRevB.66.045324

PACS number(s): 72.20.Jv, 73.21.Cd, 85.60.Bt, 42.55.Px

I. INTRODUCTION

Antimonide heterostructures, based on GaSb, InAs, AlSb, and related alloys, are of key interest for applications to infrared optoelectronics both for infrared detectors,^{1,2} and for midinfrared sources,³ in particular band-gap semiconductor lasers.⁴ The wide range of achievable band-gaps as well as band alignment, going from type I to broken gap type II or type III, provide flexibility for device engineering.⁵

The main goal of band gap engineering in midinfrared lasers is to reduce the threshold for a given emission wavelength at a given temperature. This requires a reliable model for the electronic structure of the heterostructure to fix the radiative transition energies and to maximize the strengths of the lasing transitions. Second, the nonradiative recombinations and spontaneous emission in other modes have to be taken into account and minimized to the extent possible. Since the Auger recombination mechanism becomes very important in small-band-gap lasers, the influence of a superlattice on the Auger recombination rate has become of great interest. A strong dependence of the Auger recombination on the structure would open the way for clever designs in which the recombination rate could be engineered together with other ingredients of the laser structure, leading to a further reduction of threshold and improved performance. This strategy has been pursued most consequentially by Olesberg *et al.*⁶ for InAs/GaSb active layer lasers, and most recent interband lasers have been fabricated in this system.⁷⁻¹⁰ Another combination that has been much studied is InAsSb/InAs.¹¹⁻¹³

Although lasers show an undeniable progress, unambiguous experimental evidence of the structural dependence of the Auger rate is not simple to obtain because of the necessarily indirect determination of the Auger recombination which is never present alone but always in competition with other recombination mechanisms, even in bulk samples. Values claimed for the Auger coefficient in the literature range from not very sensitive to an improvement of almost two orders of magnitude over bulk coefficients for similar effective gaps.

On the theoretical side the problem is not simple either, because the energy conservation becomes very complicated when the anisotropy and nonparabolicity of the (mini)bands are considered; at the same time it is necessary to take into

account the overlap of the wave functions of electrons entering into each recombination process. The greatest effort for bulk narrow gap materials was made by Beattie and White.¹⁴ For superlattices much work has been published for GaInSb/InAs systems,^{7,15} and for the InAsSb/InAs system a study was made by Hjalmarson and Kurtz.¹⁶ Still, in these works no genuine comparison of different heterostructures and bulk alloys has been made. Thus there is a need for reexamining the question of how much can be obtained by band-gap engineering for a reduction of the Auger coefficient. We also believe it is necessary to take into account to the greatest extent possible the details of all the recombination mechanisms, including the band structure and wave functions as close to realistic as possible, and to make sure the sum over different processes includes all non-negligible terms.

In this work we have developed a model for superlattice wave functions which we use to calculate the Auger recombination of several InAsSb-based superlattices. We compare the results among the superlattices, and compare with bulk Auger recombination rates in InAs_{1-x}Sb_x alloys calculated with the same model. The paper first presents the model for bulk band structure and Auger recombination in Secs. II and III. Then the model is extended to superlattices in Secs. IV and V. To the extent possible, theoretical results of the models on the band structure are validated by comparisons with experimental results.

II. BULK BAND-STRUCTURE MODEL

The calculation of properties of type-II superlattices requires, as a first step, a reliable description of the band structure and the wave functions. For doing this, an 18-band $k \cdot p$ method has been developed. It has three steps: a bulk $k \cdot p$ description of the constituent materials, a determination of strains in the layers with concomitant band discontinuities, and an envelope function description of the wave functions in the superlattice. We first treat the bulk model.

For a bulk material we employ a $k \cdot p$ description taking into account the (counting spins) six $\Gamma_7 - \Gamma_8$ valence bands, the two Γ_6 conduction bands, the six $\Gamma_7 - \Gamma_8$ higher-lying conduction bands, and four Γ_3 bands. The inclusion of these and only these 18 bands insures that all relevant symmetries (see Ref. 17, in particular p. 76) are included in a $k \cdot p$ matrix

TABLE I. Matrix elements of $\mathbf{k}\cdot\mathbf{p}$.

$\mathbf{k}\cdot\mathbf{p}$	A	B
X	$-\frac{1}{2}iRk_x$	$\frac{\sqrt{3}}{2}iRk_x$
Y	$-\frac{1}{2}iRk_y$	$-\frac{\sqrt{3}}{2}iRk_y$
Z	iRk_z	0

which has elements that are all *linear* in \mathbf{k} .

Compared to the conventional 14-band $\mathbf{k}\cdot\mathbf{p}$ method, we also have to calculate the matrix elements coupling the valence bands and the Γ_3 bands. Apart from spin, the Γ_3 bands are doubly degenerate, and they transform as

$$A: z^2 - \frac{1}{2}(x^2 + y^2), \quad (1)$$

$$B: x^2 - y^2, \quad (2)$$

so if we define the matrix element between the $\langle X|$ wave function of the valence band and the Γ_3 wave functions as

$$\langle X|p_x|A\rangle = -\frac{1}{2}iR, \quad (3)$$

$$\langle X|p_x|B\rangle = \frac{\sqrt{3}}{2}iR, \quad (4)$$

we obtain the rest of the matrix elements shown in Table I.

The spin-orbit splitting groups the six valence-band wave functions into heavy holes, light holes, and spin-orbit separated holes, so from the standard combination which results, using the notation of, e.g., Ref. 18, we obtain the matrix elements shown in Table II.

Since the Γ_3 bands are included only to enable enough parameters to describe the anisotropy of the hole bands closely we neglect couplings between the Γ_3 bands and other bands.

It may seem that we have greatly complicated our model by this addition, but in any model we have to diagonalize a matrix numerically, so the ease and security of programming matrix elements that are all linear in \mathbf{k} rather than folding higher-lying bands into a matrix of lower rank but nonlinear in \mathbf{k} in our opinion outweighs the extra numerical work submitted to the computer. We may further hope that the band structure and, more importantly, wave functions calculated away from the immediate neighborhood of the center of the Brillouin zone are more realistic than in a reduced $\mathbf{k}\cdot\mathbf{p}$ scheme. We emphasize that this model provides a remarkably good quantitative description of the InAsSb bulk absorption spectrum.²

This model has nine parameters: the five band energies at the center of the Brillouin zone and the four independent matrix elements of \mathbf{p} coupling the valence band to the lowest conduction band (P^2), the lowest conduction band to $\Gamma_7 - \Gamma_8$ higher-lying conduction bands (P'^2), the valence band to $\Gamma_7 - \Gamma_8$ higher-lying conduction bands (Q^2), and the valence band to the Γ_3 band (R^2). Where possible, the energies are taken from the literature,¹⁹ and the matrix elements are varied to fit the effective masses of electrons in the lowest conduction band, heavy holes in directions (100) and (111), light holes in directions (100) and (111), and holes in the spin-orbit split-off band. For the most important III-V semiconductors the gap and matrix elements together with the calculated effective masses are summarized in Table III (at $T=0$ K).

III. AUGER RECOMBINATION IN $\text{InAs}_{1-x}\text{Sb}_x$

Before we study the influence of superlattices, we calculate the Auger recombination rates for the $\text{InAs}_{1-x}\text{Sb}_x$ alloys, which are interesting in their own right, but which also serve as a reference for comparison with recombination rates in superlattice structures of similar band gaps. We recall the basic Auger processes in Fig. 1. For the CHCC process, an electron in state \mathbf{k}_l recombines with a hole in state \mathbf{k}_h and the energy gained is taken up by exciting another electron from

TABLE II. Matrix elements of $\mathbf{k}\cdot\mathbf{p}$ including spin-orbit splitting.

$\frac{1}{R}\mathbf{k}\cdot\mathbf{p}$	A \uparrow	A \downarrow	B \uparrow	B \downarrow
HH \uparrow	$-\frac{1}{2\sqrt{2}}(ik_x + k_y)$	0	$\frac{\sqrt{3}}{2\sqrt{2}}(ik_x - k_y)$	0
HH \downarrow	0	$-\frac{1}{2\sqrt{2}}(ik_x - k_y)$	0	$\frac{\sqrt{3}}{2\sqrt{2}}(ik_x + k_y)$
LH	$-\frac{1}{2\sqrt{6}}(ik_x - k_y)$	$\sqrt{\frac{2}{3}}ik_z$	$\frac{1}{2\sqrt{2}}(ik_x + k_y)$	0
LH	$-\sqrt{\frac{2}{3}}ik_z$	$-\frac{1}{2\sqrt{6}}(ik_x + k_y)$	0	$\frac{1}{2\sqrt{2}}(ik_x - k_y)$
SO \uparrow	$\frac{1}{2\sqrt{3}}(ik_x - k_y)$	$\frac{1}{\sqrt{3}}ik_z$	$-\frac{1}{2}(ik_x + k_y)$	0
SO \downarrow	$-\frac{1}{\sqrt{3}}ik_z$	$\frac{1}{2\sqrt{3}}(ik_x + k_y)$	0	$-\frac{1}{2}(ik_x - k_y)$

TABLE III. Band energies and square of independent matrix elements of \mathbf{p} used in the 18-band model (top). Effective masses calculated in the same model (bottom).

(eV)	Δ_{so}	E_g	E_7	E_8	E_3	P^2	P'^2	Q^2	R^2
AlAs	0.280	3.018	4.480	4.480	5	20.0	1.1	13.3	9.0
AlSb	0.673	2.380	3.191	3.404	5	24.0	0.0	13.0	8.7
GaAs	0.341	1.519	4.488	4.659	5	28.9	12.0	16.0	11.0
GaSb	0.760	0.810	3.191	3.404	5	25.0	6.0	14.5	9.0
InAs	0.380	0.420	4.440	4.600	5	22.2	9.0	22.0	16.0
InSb	0.810	0.237	3.160	3.490	5	24.4	10.5	16.0	11.8
(m_0)	m_{el}	$m_{HH}(100)$		$m_{HH}(111)$	$m_{LH}(100)$		$m_{LH}(111)$		m_{so}
AlAs	0.150	0.508		1.124	0.178		0.150		0.290
AlSb	0.097	0.335		0.875	0.123		0.100		0.235
GaAs	0.067	0.397		0.803	0.070		0.064		0.143
GaSb	0.041	0.290		0.758	0.045		0.041		0.140
InAs	0.023	0.257		0.456	0.026		0.025		0.082
InSb	0.014	0.256		0.585	0.014		0.014		0.101

state \mathbf{k}_2 to state \mathbf{k}_3 . Provided the two electrons and the hole are present, and the final state \mathbf{k}_3 is available, the probability rate for this process is governed by Fermi's golden rule,

$$S(\mathbf{k}_1, \mathbf{k}_2 \rightarrow \mathbf{k}_h, \mathbf{k}_3) = \frac{2\pi}{\hbar} |\langle \mathbf{k}_h, \mathbf{k}_3 | V | \mathbf{k}_1, \mathbf{k}_2 \rangle|^2 \times \delta[E(\mathbf{k}_3) + E(\mathbf{k}_h) - E(\mathbf{k}_1) - E(\mathbf{k}_2)], \quad (5)$$

in which, by virtue of the $\mathbf{k} \cdot \mathbf{p}$ approximation, the wave functions are given by the development

$$|\mathbf{k}_N\rangle = \frac{1}{\Omega} \sum_n a_n(\mathbf{k}_N) u_n(\mathbf{r}) \exp(i\mathbf{k}_N \cdot \mathbf{r}), \quad (6)$$

where u_n is the Bloch function at the center of the Brillouin zone of the n th band, and n runs over the 18 bands used in our case.

For the electron-electron interaction responsible for the process we use the statically screened Coulomb potential

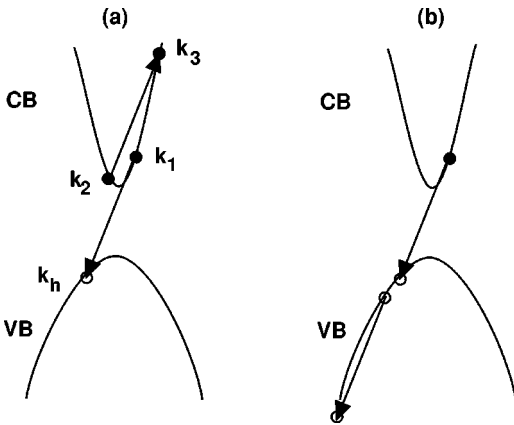


FIG. 1. The principal Auger recombination processes. (a) is a CHCC process and (b) is a CHHH process.

$$V(\mathbf{r}) = \frac{e^2 e^{-q_D r}}{4\pi\epsilon r} = \frac{1}{\Omega} \sum_q \frac{e^2/\epsilon}{q^2 + q_D^2} e^{i\mathbf{q} \cdot \mathbf{r}}, \quad (7)$$

with ϵ the permittivity and q_D the Debye (or Thomas-Fermi) wave vector

$$q_D^2 = -\frac{e^2}{\epsilon} \frac{d(p-n)}{dE_F} \quad (8)$$

for hole and electron densities p and n , respectively.

The choice of this approximation may certainly be criticized. It has been made for simplicity. An extension to dynamic screening at a finite temperature may indeed be important and perhaps feasible in a free-electron gas approximation, but taking into account the genuine dynamic permittivity of the semiconductor seems far beyond the scope of this investigation. *A fortiori* such an endeavor becomes practically prohibitive in the case of superlattices in which one should take into account all interminiband excitations. We are not aware of such work for Auger recombination. In small-band-gap materials the dominant processes will have small momentum transfers, for which the standard averaging over elementary cells then leads to an expression for the matrix element in Eq. (5),

$$\langle \mathbf{k}_h, \mathbf{k}_3 | V | \mathbf{k}_1, \mathbf{k}_2 \rangle = I_1 - I_2, \quad (9)$$

where

$$I_1(\mathbf{k}_1 \rightarrow \mathbf{k}_h, \mathbf{k}_2 \rightarrow \mathbf{k}_3) = \Delta(\mathbf{k}_2 - \mathbf{k}_3 - \mathbf{q}) \frac{1}{\Omega} \frac{e^2/\epsilon}{q^2 + q_D^2} \times \sum_{n_1} a_{n_1}^*(\mathbf{k}_h) a_{n_1}(\mathbf{k}_1) \times \sum_{n_2} a_{n_2}^*(\mathbf{k}_3) a_{n_2}(\mathbf{k}_2), \quad (10)$$

when $\mathbf{q} = \mathbf{k}_h - \mathbf{k}_1$, Δ is the Kronecker function, and

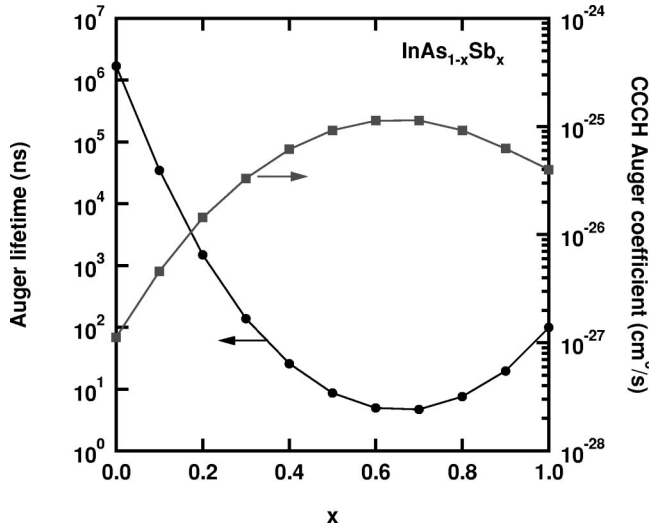


FIG. 2. Calculated intrinsic Auger lifetime and Auger coefficient for InAsSb alloys at room temperature.

$$I_2 = I_1(k_1 \rightarrow k_3, k_2 \rightarrow k_h) \quad (11)$$

is the exchange process.

The Auger recombination rate is then the weighted sum over all possible processes,

$$R = \sum_{k_1, k_2, k_h, k_3} S(k_1, k_2 \rightarrow k_h, k_3) \times f(k_1)f(k_2)[1-f(k_h)][1-f(k_3)], \quad (12)$$

where $f(k)$ is the occupation probability of state k . The momentum conservation of the matrix elements reduces the dimension of the sum to 9. The total energy conservation in principle reduces the dimension to 8, but the domain of integration is highly complex because the energy bands are neither isotropic, nor parabolic in k space.

In Fig. 2 we show our results at $T = 300$ K for the intrinsic $\text{InAs}_{1-x}\text{Sb}_x$ system. The $k \cdot p$ parameters for alloys were obtained by a linear interpolation between the binary compounds except for the fundamental gap and the spin-orbit splitting, for which experimental bowing parameters are known^{19,20} and used. As expected, the average electron lifetime defined as R/n_i varies dramatically over many orders of magnitude, mainly because of the variation of the occupation probabilities with the gap. The figure therefore also shows the intrinsic CHCC Auger coefficient $C = R/n_i^3$ which is much less dependent on the gap.

At this level of detail there are few quantitative calculations of Auger recombination in the literature. The closest is the work of Beattie *et al.*,²¹ who found an intrinsic lifetime for InSb of 43 ns. In view of the differences in constructing band structure and overlap integrals and the fact that the value is extremely sensitive to the intrinsic density, we consider the agreement between their calculation and ours very satisfactory.

We have found that for intrinsic alloys the two-hole processes can be neglected in comparison with the CHCC process. This should be borne in mind when comparing with

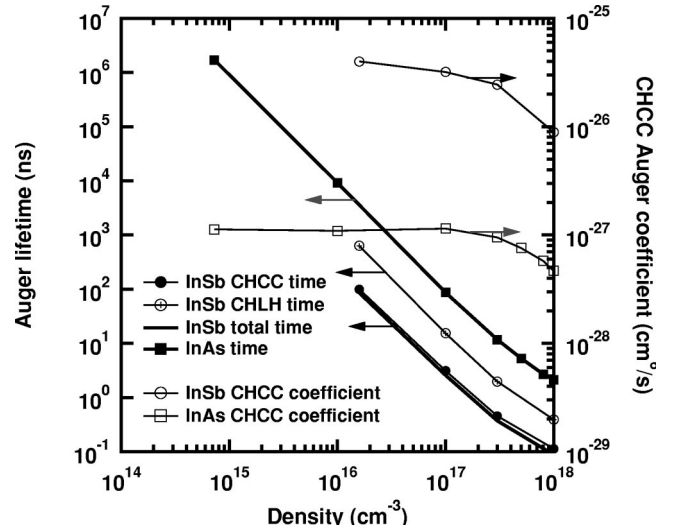


FIG. 3. Calculated Auger lifetimes and Auger coefficients for InAs and InSb as a function of electron (hole) density at room temperature.

experimental results which may not be on intrinsic samples. The most recent determinations of Auger coefficients yield $C_{Auger} = 1.1 \times 10^{-26} \text{ cm}^6/\text{s}$ (Ref. 22), and $C_{Auger} = 6 \times 10^{-27} \text{ cm}^6/\text{s}$ (Ref. 23), for InAs, $C_{Auger} = 2.1 \times 10^{-26} \text{ cm}^6/\text{s}$ (Ref. 23), for $\text{InAs}_{0.91}\text{Sb}_{0.09}$, and $C_{Auger} = 1 \times 10^{-26} \text{ cm}^6/\text{s}$ (Ref. 24), and $C_{Auger} = 7 \times 10^{-26} \text{ cm}^6/\text{s}$ (Ref. 25), for InSb. Clearly our results indicate a larger variation with alloy composition for the Auger coefficient than these values. The latter are generally larger for the As-rich alloys but smaller for InSb.

By introducing different quasi-Fermi levels for electrons and holes in Eq. (12) we can study the density dependence of the Auger lifetime. This is done in Fig. 3 for the case of equal electron and hole densities. For low densities the characteristic $1/n^2$ dependence of the average lifetime is seen; at higher (degenerate) densities the occupation of (especially) electron final states tends to reduce the dependence and thereby the effective Auger coefficient. This may explain why some experimentally measured coefficients in InSb are smaller than in the limit of nondegenerate densities.

The difference between experimental results and ours in the case of InAs can of course not be explained by this effect. We feel it is still an open question whether the discrepancy is due to approximations in our model or an indication that other types of processes—such as phonon-assisted Auger recombination—play a predominant role. We should not forget the main goal of our work, however, which is to study the possible influence of a superlattice on recombination. For this it is essential to resort to the same type of process in the bulk and superlattice cases.

IV. SUPERLATTICE BAND-STRUCTURE MODEL

We now want to extend our calculations to periodic superlattices. There are two parts to this problem: The layers in the structure will be strained, which modifies the band structure of each layer, and the sequence of layers in one period

will modify the wave functions. This creates the familiar miniband structure in a Brillouin zone which has a thickness of $2\pi/d$ in the growth direction z , where d is the period of the superlattice.

A. Band alignments in the strained superlattice

The superlattices are assumed to be perfectly epitaxial, so that the lateral lattice parameters are fixed by the substrate. Then the biaxial strain in the superlattice is determined by simple macroscopic mechanics involving the elastic moduli of the materials. From the deformation potentials we then derive the Pikus-Bir matrix elements which add to the $\mathbf{k}\cdot\mathbf{p}$ matrix.²⁶ Most contributions are just a displacement of the conduction and valence bands added to the diagonal of the matrix, but there is also a matrix element coupling the spin-orbit split-off band with the light-hole valence band. Because the influence of strain on higher-lying bands is unknown, we have kept their energies unchanged.

The band structure of a material under biaxial strain is then complicated by the lifting of the degeneracy of the heavy and light holes at the center of the Brillouin zone and the ensuing anticrossing dispersion relations.²⁷ But the mathematical problem has not changed; for each value of \mathbf{k} the problem is still that of diagonalizing an 18×18 matrix.

The remaining important parameter is the difference in (unstrained) valence band positions for a heterojunction of two materials. For this, we mainly rely on the values compiled by Tiwari and Frank²⁸ and Krijn.²⁹

B. Superlattice wave functions

For wave functions in a superlattice we use an 18-band *envelope function* approximation as follows. The growth direction is taken to be z , and \mathbf{R} is the component of \mathbf{r} in the direction parallel to the interfaces. The Hamiltonian for the system is then taken to be

$$H_{sl} = \frac{p^2}{2m_0} + V_c(\mathbf{r};z) + V_{VB}(z), \quad (13)$$

where V_c is the crystal potential for the material at position z , and V_{VB} indicates the position of the unstrained valence-band maximum energy of the material at position z relative to a common reference material. This means that heterojunction band discontinuities are considered commutative and associative.

The material at z is now characterized by its $\mathbf{k}\cdot\mathbf{p}$ matrix elements as in the bulk case described in Sec. II. This means that the Bloch wave functions $u_{i0}(\mathbf{r})$ at the center of the Brillouin zone are eigensolutions to the Hamiltonian

$$H_{bulk} = \frac{p^2}{2m_0} + V_c(\mathbf{r};z), \quad (14)$$

in which z is only a parameter. Then, by construction, the Bloch functions are orthogonal within a unit cell, and their eigenenergies and \mathbf{p} matrix elements are those given in the tables of Sec. II.

In order to solve the eigenvalue problem for the periodic superlattice

$$H_{sl}\psi_{n,\mathbf{k}} = E_n(\mathbf{k})\psi_{n,\mathbf{k}} \quad (15)$$

for a state of wave vector \mathbf{k} in the reduced Brillouin zone in miniband number n , we make the envelope-function approximation and expand the z -dependent envelope functions in a Fourier series so that the state wave function is written as

$$\psi_{n,\mathbf{k}}(\mathbf{r}) = \sum_{m,i} a_n^{mi}(\mathbf{k}) e^{i(k_z + G_m)z} e^{i\mathbf{k}_{\parallel}\cdot\mathbf{R}} u_{i0}(\mathbf{r};z), \quad (16)$$

and $G_m = 2m\pi/d$. In the sum, the index i runs over the 18 bands and m is an integer $-N_G \leq m \leq N_G$ which runs over the number of Fourier components retained. Introducing the reciprocal-lattice vectors $\mathbf{G}_m = G_m \hat{\mathbf{k}}_z$, we may write the expansion in a slightly more compact way:

$$\psi_{n,\mathbf{k}}(\mathbf{r}) = \sum_{m,i} a_n^{mi}(\mathbf{k}) e^{i(\mathbf{k} + \mathbf{G}_m)\cdot\mathbf{r}} u_{i0}(\mathbf{r};z). \quad (17)$$

Applying the superlattice Hamiltonian (13) to this wave function leads to

$$\begin{aligned} H_{sl}\psi_{n,\mathbf{k}}(\mathbf{r}) = \sum_{m,i} a_n^{mi}(\mathbf{k}) e^{i(\mathbf{k} + \mathbf{G}_m)\cdot\mathbf{r}} & \left[\frac{p^2}{2m_0} + V_c(\mathbf{r};z) \right. \\ & + V_{VB}(z) \left. \right] u_{i0}(\mathbf{r};z) + \frac{\hbar^2(\mathbf{k} + \mathbf{G}_m)^2}{2m_0} \\ & + \frac{\hbar}{m_0}(\mathbf{k} + \mathbf{G}_m)\cdot\mathbf{p} u_{i0}(\mathbf{r};z) \left. \right]. \quad (18) \end{aligned}$$

The envelope-function approximation now consists in assuming that within each elementary cell only the Bloch functions vary, all other functions being considered constant at the scale of a cell. Multiplying by $e^{-i(\mathbf{k} + \mathbf{G}_{m'})\cdot\mathbf{r}} u_{j0}^*(\mathbf{r};z)$, integrating over the whole volume, and utilizing the orthogonality of the Bloch functions within each cell, we obtain the approximation to Schrödinger equation (15) for superlattice states as the eigenvalue problem

$$\begin{aligned} \sum_{m,m',i,j} a_n^{mi}(\mathbf{k}) & \left\{ \frac{\hbar^2(\mathbf{k} + \mathbf{G}_m)^2}{2m_0} \Delta_{m,m'} \Delta_{i,j} \right. \\ & + \frac{1}{d} \int_0^d e^{i(G_m - G_{m'})z} [\epsilon_i(z) + V_{VB}(z)] dz \Delta_{i,j} + \frac{\hbar}{m_0}(\mathbf{k} \\ & + \mathbf{G}_m) \cdot \frac{1}{d} \int_0^d e^{i(G_m - G_{m'})z} \mathbf{P}_{ji}(z) dz \left. \right\} \\ & = E_n(\mathbf{k}) a_n^{jm'}(\mathbf{k}), \quad (19) \end{aligned}$$

in which \mathbf{P}_{ji} is the momentum matrix element between the Bloch states of bands i and j . In the case of a superlattice consisting of only one material, this equation can be seen to lead to the bulk $\mathbf{k}\cdot\mathbf{p}$ band structure folded into the superlattice Brillouin zone, as it should be. The equation has the usual problem that it is derived under the assumption that material changes occur slowly, but that we apply it to het-

TABLE IV. Growth parameters of the IMEC InAs/InAs_{1-x}Sb_x/InAs/Al_yIn_{1-y}As samples.

Sample	InAs		InAs _{1-x} Sb _x		Al _y In _{1-y} As	
	<i>d</i> (nm)	<i>x</i>	<i>d</i> (nm)	<i>x</i>	<i>y</i>	<i>d</i> (nm)
Q259	12.8	0.30	2.5	0.25	2.5	
Q344	10.0	0.16	2.0	0.15	2.0	
Q346	10.0	0.15	1.0	0.15	1.0	
Q347	10.0	0.16	0.5	0.15	0.5	
Q385	6.0	0.12	4.0	0.09	4.0	

erojunctions where those changes are ideally discontinuous. On the other hand, the fact that the coupling between bands is only linear in k conveniently avoids—or covers up—questions about particular connection rules at an interface.³⁰ These questions can hardly be solved without a model on an atomic length scale, and they will not be considered here. We simply apply the approximations and check with experiments that the model seems to predict reasonably correct results.

With these assumptions the Schrödinger equation for the miniband state [Eq. (19)] is a standard eigenvalue problem for the coefficients $a_n^{mi}(\mathbf{k})$ with a super- $k \cdot p$ matrix of size $18(2N_G + 1) \times 18(2N_G + 1)$ for each \mathbf{k} in the miniband Brillouin zone. A brute force diagonalization of this matrix then leads to the miniband energies and wave functions.

C. Results for type-II superlattices

In an earlier publication³¹ we showed several results for strained InAs/AlSb superlattices grown on GaSb. Excellent agreement between experimental absorption spectra, including their polarization dependence, was found.

Here we compare the experimental and theoretical effective band gaps (energy difference between lowest-lying electron and highest-lying hole states) of several more complicated four layers-per-period samples of InAs/InAs_{1-x}Sb_x/InAs/Al_yIn_{1-y}As on InAs substrates. The compositions of the alloys were chosen to equilibrate compressive and tensile stress in each period. These samples were fabricated and characterized at IMEC,³² Leuven, Belgium, and the main characteristics are given in Table IV.

For illustration, in Fig. 4 we show the valence and conduction bands as well as the position of the miniband levels at the center of the Brillouin zone calculated for the most strained structure Q259. With our parameters, the structure is clearly of type II. For the other samples the InAs_{1-x}Sb_x conduction band is so close to the InAs conduction band that it makes no meaning to classify the structure as type I or type II. The comparison between photoluminescence results and the theoretical effective band gap is shown in Fig. 5. The difference is in the 10-meV range for all the structures, which increases our confidence in the envelope function model.

V. AUGER RECOMBINATION IN SUPERLATTICES

The Auger recombination in a superlattice can now be evaluated by extending the theory of Sec. III to transitions

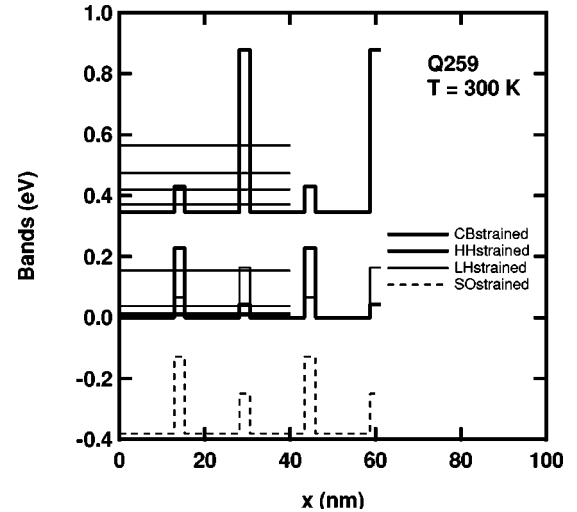


FIG. 4. Calculated band profile for sample Q259. Also shown are the positions of the pertinent miniband states at the center of the Brillouin zone.

between miniband states. For each transition corresponding to a *recombination process* the initial state will consist of two particles of the same type (both in conduction minibands or both in valence minibands) k_1 and k_2 in minibands N_1 and N_2 , respectively, and the final state will consist of two particles of opposite type k_3 and k_4 in minibands N_3 and N_4 , respectively.

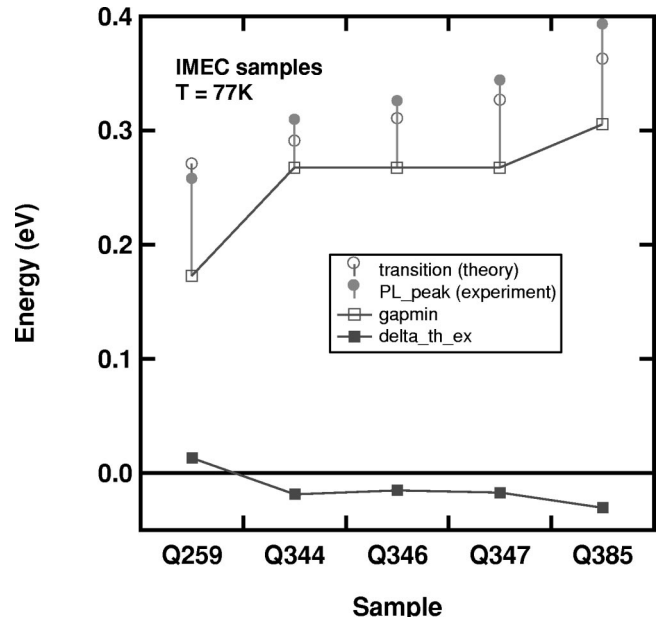


FIG. 5. Comparison of the theoretical $e1-h1$ transition energy and the experimental photoluminescence energy. “gapmin” represents the difference between the minimum of the conduction-band profile and the maximum of the valence-band profiles. The difference between theory and experiment, marked “delta_th_ex” can be seen to be satisfactorily small even though the confinement energies vary considerably.

A. Theory

The interaction is still the screened Coulomb interaction [Eq. (7)], but the wave functions and energies entering the Fermi golden rule, [Eq. (5)] are those of the superlattice described by the coefficients $a_{N_1}^{m_1 i_1}(\mathbf{k}_1)$, etc., of expansion (17) determined from Eq. (19).

Consistent with the envelope-function approximation, we can calculate the corresponding matrix element for the process by averaging over elementary cells and employing the orthogonality of the center-of-zone Bloch functions. Apart from handling the great increase in number of indices, we also have to include “umklapp” transitions in the much smaller Brillouin zone. The final result is analogous to Eqs. (9)–(11),

$$\langle \mathbf{k}_3, \mathbf{k}_4 | V | \mathbf{k}_1, \mathbf{k}_2 \rangle = I_1 - I_2, \quad (20)$$

where

$$\begin{aligned} I_1(\mathbf{k}_1 \rightarrow \mathbf{k}_3, \mathbf{k}_2 \rightarrow \mathbf{k}_4) &= \sum_{m_1 m_2 m_3 m_4} \Delta[\mathbf{k}_2 - \mathbf{k}_4 - \mathbf{q}_0 + \mathbf{G}_1(m_1 - m_3 + m_2 - m_4)] \\ &\times \frac{1}{\Omega} \frac{e^2/\epsilon}{[\mathbf{q}_0 - \mathbf{G}_1(m_1 - m_3)]^2 + q_D^2} \\ &\times \sum_{i_1} a_{N_3}^{m_3 i_1^*}(\mathbf{k}_3) a_{N_1}^{m_1 i_1}(\mathbf{k}_1) \sum_{i_2} a_{N_4}^{m_4 i_2^*}(\mathbf{k}_4) a_{N_2}^{m_2 i_2}(\mathbf{k}_2), \end{aligned} \quad (21)$$

where $\mathbf{q}_0 = \mathbf{k}_3 - \mathbf{k}_1$, $\mathbf{G}_1 = (2\pi/d)\hat{\mathbf{k}}_z$, Δ is the Kronecker function, and

$$I_2 = I_1(\mathbf{k}_1 \rightarrow \mathbf{k}_4, \mathbf{k}_2 \rightarrow \mathbf{k}_3) \quad (22)$$

is the exchange process again.

The Auger recombination rate for a given quadruple of minibands (N_1, N_2, N_3, N_4) is then the weighted sum over all possible processes within the reduced Brillouin zone,

$$\begin{aligned} R_{N_1 N_2 N_3 N_4} &= \sum_{\mathbf{k}_1, \mathbf{k}_2, \mathbf{k}_3, \mathbf{k}_4} S(\mathbf{k}_1, \mathbf{k}_2 \rightarrow \mathbf{k}_3, \mathbf{k}_4) \\ &\times f(\mathbf{k}_1) f(\mathbf{k}_2) [1 - f(\mathbf{k}_3)] [1 - f(\mathbf{k}_4)], \end{aligned} \quad (23)$$

with S the transition rate [Eq. (5)], and the total rate is the sum over minibands fulfilling the condition mentioned above to assure that the process is an *interband* recombination process. Clearly, many miniband transitions give a negligible contribution to the Auger recombination rate, so strategies have been employed to evaluate only those that are of importance in the total recombination rate.

B. Results

We have calculated the average Auger recombination rate for the IMEC superlattices discussed above (Table IV). As we saw in Sec. IV C, those samples are well described by our

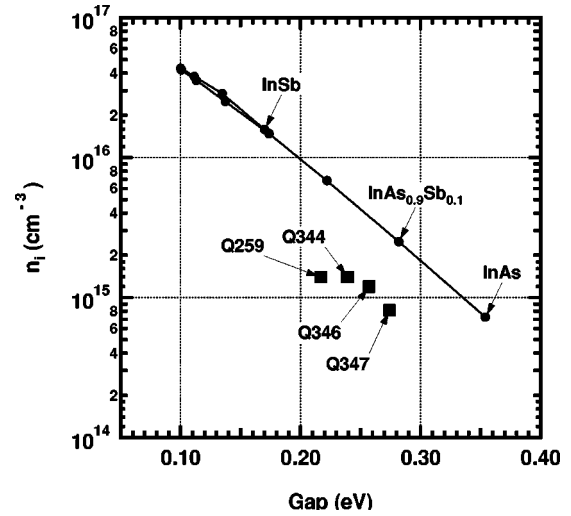


FIG. 6. Comparison of the intrinsic density for the IMEC superlattices with that of bulk InAsSb alloys vs the (effective) gap. $T = 300$ K.

wave functions at $T = 77$ K and they also span a number of cases from strongly strained (Q259) to less strained and several thicknesses.

We compare our results to the bulk results obtained in Sec. III at room temperature and at intrinsic densities. It is very important to decide what to compare.

In Fig. 6 we show the intrinsic density of the superlattices compared with bulk alloys as a function of the effective gap. As one could expect, essentially the smaller the filling factor of the superlattices, the smaller the intrinsic density.

The intrinsic densities naturally depend strongly on the effective gap, and so does the Auger rate. But a major dependence of the Auger rate comes from the electron and hole densities. One should therefore certainly compare bulk and superlattices having the same gap. However, the Auger recombination rate at intrinsic densities is not of much interest either, since the superlattices generally have smaller intrinsic densities than bulk samples of the same gap. Finally, the Auger recombination is mainly an obstacle to achieving low thresholds in lasers, so the most relevant comparison is the Auger coefficient as a function of the *effective gap*.

The main results of this work are therefore summarized in Fig. 7. This figure contains, first, the results for bulk alloys already presented in Fig. 2 for reference. Second, the calculated results for the IMEC superlattices at low density are shown as squares with sample number tagged on.

The first conclusion that can be drawn is that for the superlattices the Auger coefficient does not vary much with the structure, and is rather close to the bulk values for equivalent gaps. The calculations do not predict a large decrease in coefficient. Second, the strongest reduction is found for the most strained superlattice Q259, whose structure was presented in Fig. 4. The latter figure also shows that the hole miniband structure of that sample shows a strong separation between the highest-lying miniband (with a concentration of the wave function in the InAsSb layer) and lower-lying hole minibands. This reduces the hole density of states in a larger energy interval just below the gap, and leads to a reduction

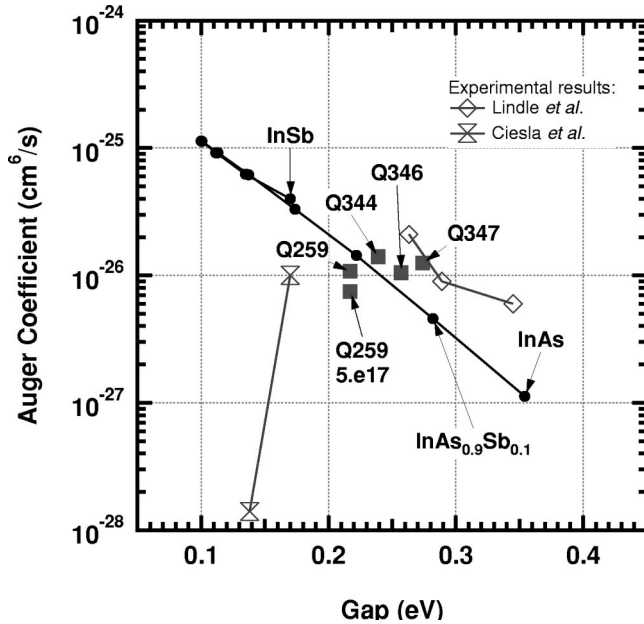


FIG. 7. Comparison of the intrinsic Auger coefficient for the IMEC superlattices with that of bulk InAsSb alloys vs the (effective) gap. $T=300$ K. Also shown are some experimental results from the literature. The result marked 5.e17 represents the calculated Auger coefficient for an average electron (hole) density of $5 \times 10^{17} \text{ cm}^{-3}$, and illustrates the reduction of the coefficient with increasing density as observed in the bulk (see Fig. 3).

of the population of holes available for recombination in lower-lying minibands. Then the predominant channel for recombination is between the $e1$ and $h1$ minibands.

For less-strained samples the hole confinement in the InAsSb layer is smaller, so the $h1$ miniband is much closer to the “continuum” InAs valence band. In this case the lower-lying minibands contribute considerably to the Auger recombination, and many different quadruples of minibands in Eq. (23) have to be included in the total Auger recombination rate. This interpretation is corroborated by the tendency between samples Q344, Q346, and Q347, in which the thickness of the InAsSb layers decreases, gradually pushing the $h1$ miniband closer and closer to the “continuum” and gradually involving more and more channels to the summed Auger recombination coefficient. A strategy for obtaining the lowest possible Auger coefficient would therefore be to choose as strong a strain as possible, followed by a thickness of the hole-confining layer such as to keep the fundamental hole state as far from lower-lying states (including “continuum” states) as possible. But one cannot expect very spectacular reductions in the coefficient at room temperature. It is worth noting that this strategy is not different from the strategy one employs to reduce the transparency threshold *density* for a laser structure; in fact the latter reduction may be much more important for laser performance than a possible reduction of Auger coefficient.

For InAsSb superlattices there are few experimental results available in the literature. In the figure we show (diamonds) results of Lindle *et al.*²³ comparing Auger rates for a superlattice (midpoint) with that of bulk alloys. We have

shifted the gap relative to the 77 K values indicated in their paper to take into account the expected reduction of gaps at $T=300$ K. The absolute values of the Auger coefficients are all higher than found theoretically, but the dependency on gap agrees well for the bulk alloys. For the superlattice a modest reduction is found, in quite reasonable agreement with what can be expected from our theory.

Finally, we have included the results of Ciesla *et al.*²⁴ who measured the Auger coefficient of InSb and that of an InAs/InAs_{0.68}Sb_{0.32} superlattice on an InAs_{0.84}Sb_{0.16} relaxed buffer (sample IC389). They found an improvement of about two orders of magnitude, which definitely is not predicted by our theory. A few remarks are called for. First, our parameters for the valence-band offsets are different from those used by Ciesla *et al.*: our parameters place the conduction band of the InAs_{0.68}Sb_{0.32} alloy below the conduction band of InAs, whereas theirs led to the opposite order (also see the discussion of this point in Ref. 33). However, whether we use our parameters or theirs we find—as they did and measured—an effective gap of the superlattice quite close to that of InSb. Second, their experiment relied on a bleaching pulse of energy about twice the gap in either case and of sufficient intensity to obtain total bleaching. The crucial point is now that the experiment measures essentially the decrease of the bleaching gap (the difference between quasi-Fermi energies of electrons and holes) as a function of time after total bleaching. In order to extract a recombination rate it is then necessary to convert the bleaching gap to the electron-hole density, which requires some model. If we take a quasi-Fermi energy difference of around 270 meV, our model gives an electron (hole) density of $8 \times 10^{17} \text{ cm}^{-3}$ for bulk InSb, $4 \times 10^{17} \text{ cm}^{-3}$ for the superlattice using our parameters, and $6 \times 10^{17} \text{ cm}^{-3}$ using the band offset rule preferred by Smith *et al.*³⁴ While the density for InSb agrees well with the maximum density of the bleaching experiment, it seems impossible to reconcile the model results with the densities of almost 10^{19} cm^{-3} employed in the extraction²⁴ of the Auger coefficient for the superlattice. This would require a much higher electron density-of-states, corresponding to an electron density of states mass considerably larger than the masses of either constituent material. We therefore feel that the spectacular reduction of the Auger coefficient to a great extent has its origin in the problematic assignment of electron-hole plasma densities.

VI. CONCLUSION

The $k \cdot p$ model we have presented has shown very satisfactory agreement with various experimental results such as optical-absorption spectra in both bulk narrow-gap semiconductors and in narrow-gap superlattices. We are therefore confident in the description of the states it delivers. For the Auger recombination the experimental data are sparse and the comparison with our results is not conclusive. It is not clear whether this is due to experimental difficulties or to insufficiency of our model.

Theoretically, the influence of the superlattice structure has been quantitatively evaluated and a strategy for minimizing the Auger coefficient has been suggested. We conclude,

however, that since the design strategy for reducing the threshold density in a laser based on these superlattices would be the same even if there were no superlattice effect on the Auger coefficient, it will remain difficult to attribute improvements of such lasers to an improvement in the Auger recombination coefficient.

ACKNOWLEDGMENTS

This work was partially supported by the European Union via Contract No. AIR. The author particularly thanks one of the contract partners IMEC for permission to use unpublished results on their structures in this paper.

*Email address: borge.vinter@thalesgroup.com

- ¹D.L. Smith and C. Mailhot, *J. Appl. Phys.* **62**, 2545 (1987).
- ²A. Rakovska, V. Berger, X. Marcadet, B. Vinter, K. Bouzehouane, and D. Kaplan, *Semicond. Sci. Technol.* **15**, 34 (2000).
- ³*Long Wavelength Infrared Emitters Based on Quantum Wells and Superlattices*, edited by M. Helm, Optoelectronic Properties of Semiconductor Superlattices Vol. 6 (Gordon and Breach, Amsterdam, 2000).
- ⁴H. K. Choi and G. W. Turner, in *Long Wavelength Infrared Emitters Based on Quantum Wells and Superlattices (Ref. 3)*, pp. 225–305.
- ⁵R. Q. Yang, in *Long Wavelength Infrared Emitters Based on Quantum Wells and Superlattices (Ref. 3)*, pp. 13–64.
- ⁶J.T. Olesberg, M.A. Flatté, T.C. Hasenberg, and C.H. Grein, *J. Appl. Phys.* **89**, 3283 (2001).
- ⁷M.E. Flatté, J.T. Olesberg, S.A. Anson, T.F. Boggess, T.C. Hasenberg, R. Miles, and C.H. Grein, *Appl. Phys. Lett.* **70**, 3212 (1997); **74**, 188 (1999).
- ⁸I. Vurgaftman, J.R. Meyer, F. Julien, and L.R. Ram-Mohan, *Appl. Phys. Lett.* **73**, 711 (1998).
- ⁹J.R. Meyer, C.L. Felix, W.W. Bewley, I. Vurgaftman, E.H. Aifer, J.L. Olafsen, J.R. Lindle, C.A. Hoffman, M.-J. Yang, H. Lee, C.-H. Lin, and S.S. Pei, *Appl. Phys. Lett.* **73**, 2857 (1998).
- ¹⁰W.W. Bewley, H. Lee, I. Vurgaftman, R.J. Menna, C.L. Felix, R.U. Martinelli, D.W. Stokes, D.Z. Garbuzov, J.R. Meyer, M. Maiorov, J.C. Connolly, and A.R. Sugg, *Appl. Phys. Lett.* **76**, 256 (2000).
- ¹¹A. Wilk, M. El Gazouli, M. El Skouri, P. Christol, P. Grech, and A.N. Baranov, *Appl. Phys. Lett.* **77**, 2298 (2000).
- ¹²S.R. Kurtz, R.M. Biefeld, A.A. Allerman, A.J. Howard, M.H. Crawford, and M.W. Pelczynski, *Appl. Phys. Lett.* **68**, 1332 (1996).
- ¹³A.A. Allerman, R.M. Biefeld, and S.R. Kurtz, *Appl. Phys. Lett.* **69**, 465 (1996).
- ¹⁴A.R. Beattie and A.M. White, *J. Appl. Phys.* **79**, 802 (1996).
- ¹⁵D.-J. Jang, M.E. Flatté, C.H. Grein, J.T. Olesberg, T.C. Hasenberg, and T.F. Boggess, *Phys. Rev. B* **58**, 13 047 (1998).
- ¹⁶H.P. Hjalmarson and S.R. Kurtz, *Appl. Phys. Lett.* **69**, 949 (1996).
- ¹⁷P. Y. Yu and M. Cardona, *Fundamentals of Semiconductors: Physics and Materials Properties* (Springer-Verlag, Berlin, 1996).
- ¹⁸C. Hermann and C. Weisbuch, *Phys. Rev. B* **15**, 823 (1977).
- ¹⁹*Semiconductors-Basic Data* 2nd ed., edited by O. Madelung (Springer-Verlag, Berlin, 1996).
- ²⁰O. Berolo and J. C. Woolley, in *Proceedings of the 11th International Conference on the Physics of Semiconductors*, edited by M. Miasek (Polish Scientific Publishers, Warszawa, 1972), Vol. 2, pp. 1420–25.
- ²¹A.R. Beattie, R.A. Abram, and P. Scharoch, *Semicond. Sci. Technol.* **5**, 738 (1990).
- ²²K.L. Vodopyanov, H. Graener, C.C. Phillips, and T.J. Tate, *Phys. Rev. B* **46**, 13 194 (1992).
- ²³J.R. Lindle, J.R. Meyer, C.A. Hoffmann, F.J. Bartoli, G.W. Turner, and H.K. Choi, *Appl. Phys. Lett.* **67**, 3153 (1995).
- ²⁴C.M. Ciesla, B.N. Murdin, C.R. Pidgeon, R.A. Stradling, C.C. Phillips, M. Livingstone, I. Galbraith, D. Jaroszynski, C.J.G.M. Langerak, P.J.P. Tang, and M.J. Pullin, *J. Appl. Phys.* **80**, 2994 (1996).
- ²⁵S. Marchetti, M. Martinelli, and R. Simili, *J. Phys.: Condens. Matter* **13**, 7363 (2001).
- ²⁶G. E. Pikus and G. L. Bir, *Symmetry and Strain Induced Effects in Semiconductors* (Wiley, New York, 1974).
- ²⁷S.L. Chuang, *Phys. Rev. B* **43**, 9649 (1990).
- ²⁸S. Tiwari and D.J. Frank, *Appl. Phys. Lett.* **60**, 630 (1992).
- ²⁹M.P.C.M. Krijn, *Semicond. Sci. Technol.* **6**, 27 (1991).
- ³⁰B.A. Foreman, *Phys. Rev. B* **54**, 1909 (1996).
- ³¹I. Prevot, B. Vinter, F.H. Julien, F. Fossard, and X. Marcadet, *Phys. Rev. B* **64**, 195318 (2001).
- ³²L. Song and P. Heremans (private communication).
- ³³I. Vurgaftman, J.R. Meyer, and L.R. Ram-Mohan, *J. Appl. Phys.* **89**, 5815 (2001).
- ³⁴S.N. Smith, C.C. Phillips, R.H. Thomas, R.A. Stradling, I.T. Ferguson, A.G. Norman, B.N. Murdin, and C.R. Pidgeon, *Semicond. Sci. Technol.* **7**, 900 (1992).